Article

Not peer-reviewed version

Mutations in the TRS Region Alter Coronavirus (Porcine Epidemic Diarrhea Virus) Replication and Interferon Induction by Modulating Subgenomic RNA Transcription

Mingde Liu , Jelmer W. Poelstra , Shaomin Yang , Qiuhong Wang *

Posted Date: 15 September 2025

doi: 10.20944/preprints202509.1182.v1

Keywords: coronavirus; porcine epidemic diarrhea virus; nidovirus; transcriptional regulatory sequence; subgenomic RNA; sgmRNA; discontinuous transcription; interferon

 doi:10.20944/preprints202509.1182.v1

Article

Mutations in the TRS Region Alter Coronavirus (Porcine Epidemic Diarrhea Virus) Replication and Interferon Induction by Modulating Subgenomic RNA Transcription

Mingde Liu [1,2], Jelmer W. Poelstra [3], Shaomin Yang [4] and Qiuhong Wang [1,2,*]

[1] Center for Food Animal Health, Department of Animal Sciences, College of Food, Agricultural and Environmental Sciences, The Ohio State University, Wooster, OH, USA
[2] Department of Veterinary Preventive Medicine, College of Veterinary Medicine, The Ohio State University, Columbus, OH, USA
[3] Molecular and Cellular Imaging Center (MCIC), The Ohio State University, Wooster, OH, USA
[4] Department of Pain Medicine, Shenzhen Nanshan People's Hospital and the 6th Affiliated Hospital of Guangdong Medical University, Shenzhen, China
* Correspondence: wang.655@osu.edu

Abstract

Coronaviruses frequently cause epidemics of respiratory or enteric disease in humans and livestock. CoVs generate a nested set of subgenomic messenger RNAs (sgmRNAs) through discontinuous transcription mediated by transcription regulatory sequences (TRSs). We previously developed a porcine epidemic diarrhea virus (PEDV) mutant, RMT, by remodeling TRS-core sequences (TRS-CSs). Unexpectedly, plasmid mutagenesis introduced a 189-nucleotide insertion upstream of the E gene TRS-CS and a guanine deletion in the N gene TRS-CS. RMT displayed markedly increased sgmRNA-E transcription, which is normally the least abundant in wild-type PEDV. To assess the effects of TRS remodeling and the additional mutations, we generated PEDV mutants with various modification combinations and characterized them in vitro. TRS-CS remodeling alone impaired replication, reduced sgmRNA-N abundance, and increased non-canonical transcription, which correlated with strong interferon responses. The insertion upstream of E gene TRS-CS enhanced sgmRNA-E transcription in a size-dependent manner, with the 189-nt insertion more effective than 94-nt insertion. The 189-nt insertion also boosted other canonical sgmRNA transcription, reduced transcriptional noise and partially restored replication, while the 94-nt insertion did not. These results demonstrate that TRS-CSs and their flanking sequences critically regulate CoV transcription, replication, and immune responses, providing insights for designing recombination-resistant live attenuated vaccines through TRS remodeling.

Keywords: coronavirus; porcine epidemic diarrhea virus; nidovirus; transcriptional regulatory sequence; subgenomic RNA; sgmRNA; discontinuous transcription; interferon

1. Introduction

Coronaviruses (CoVs), members of the *Coronavirinae* subfamily within the *Coronaviridae* family in the *Nidovirales* order, are enveloped, positive-sense RNA viruses that infect a wide range of host species, including mammals and birds [1,2]. Over the past two decades, multiple highly pathogenic CoVs, such as severe acute respiratory syndrome coronavirus (SARS-CoV) [3], Middle East respiratory syndrome coronavirus (MERS-CoV) [4], and potentially SARS-CoV-2 [5–7], have emerged from wildlife reservoirs, leading to epidemics/pandemics in humans with considerable morbidity, mortality, and economic impact. These viruses spread rapidly, cause substantial disease,

 doi:10.20944/preprints202509.1182.v1

and can cross species barriers, emphasizing the critical need for deeper insights into CoV replication and its life cycle [8]. Porcine epidemic diarrhea virus (PEDV), a member of the Alphacoronavirus genus, is a major enteric pathogen of pigs [9–11]. It infects pigs of all ages and causes porcine epidemic diarrhea (PED) characterized by acute diarrhea, vomiting, dehydration, and even death. Neonatal piglets are most susceptible to PEDV with up to 100% mortality [11–19]. During the early stages of infection, innate immune responses, particularly interferons (IFNs), play a critical role in controlling viral infections by initiating antiviral signaling pathways and shaping the host's defense. A deeper understanding of the molecular mechanisms governing CoV transcription and replication, as well as their interaction with host IFN responses, is essential for informing the development of effective antiviral therapeutics and vaccines. In this study, we used PEDV as a model to study the conserved mechanisms of CoV replication and transcription [20].

Similar to other CoVs, the 28-kb long PEDV genome is arranged in the order of 5′ untranslated region (UTR)-ORF1a-ORF1b-ORF of spike (S) protein -ORF3-ORF of envelop (E) protein-ORF of membrane (M) protein-ORF of nucleocapsid (N) protein-3′UTR-polyA [21–24]. ORF1a and ORF1b encode polyproteins that are cleaved into 16 nonstructural proteins (nsp1 - nsp16). The remaining ORFs encode four structural proteins (S, E, M, and N proteins) and one accessory protein ORF3. Like other CoVs, PEDV utilizes a unique discontinuous transcription mechanism to generate a nested set of 5′- and 3′-co-terminal negative-sense (-) subgenomic (sg) RNAs [25–28]. These (-) sgRNAs serve as templates for the transcription of positive-sense subgenomic messenger RNAs (sgmRNAs) that encode structural and accessory proteins (Figure 1A).

Discontinuous transcription is regulated by transcription regulatory sequences (TRSs), composed of a conserved core sequence (CS) flanked by variable flanking sequences [29–32]. A single leader TRS (TRS-L) is located at the 5′ UTR, while body TRSs (TRS-Bs) are positioned upstream of each structural or accessory gene. During negative-strand synthesis, when the RNA-dependent RNA polymerase (RdRp) reads through the PEDV genomic RNA (gRNA), it may transiently pause at TRS-B. At this point, the polymerase either continues reading through to the next gene or switches templates to the TRS-L, generating a shorter (-)sgRNA. These (-)sgRNAs serve as templates for the production of canonical sgmRNAs (Figure 1A). In addition to these canonical sgmRNAs, deep sequencing data has revealed the existence of numerous non-canonical transcripts with unclear functions [33–35].

Previously, our lab has generated an infectious clone for PEDV strain PC22A [22] and replaced the ORF3 of PC22A with the enhanced green fluorescent protein (EGFP) gene and generated an infectious clone-derived reporter virus, dORF3-EGFP [21]. Recently, we used dORF3-EGFP as the backbone and engineered a recombination-resistant mutant, called RMT (Figure 1B), carrying recoded TRS-CSs in front of all ORFs except for EGFP [36]. The rewired TRS-CS in RMT is incompatible with the wild-type TRS-CS in all field PEDV strains, preventing the generation of recombined infectious progeny between RMT and any wild-type PEDV. However, two unexpected mutations were identified in the rescued RMT virus: 1) a 189-nucleotide (nt) insertion containing four repetitive sequences upstream of the E gene TRS-CS, and 2) a guanine (G) deletion in the 5′-end of N gene TRS-CS (Figure 1B). These mutations were introduced during plasmid mutagenesis. RNA sequencing (RNA-seq) of the total RNA extracted from the small intestinal contents (SIC) of the RMT-infected gnotobiotic pigs uncovered a notable alteration in the sgmRNA transcription profile, with sgmRNA-E surpassing sgmRNA-N abundance, deviating from the typical transcription profile of wild-type PEDV. In a more recent study, we fixed these two unexpected mutations in RMT and further deleted the EGFP gene to generate RMTv1 mutant [37]. We found that RMTv1 replicated less efficiently in vitro and induced significantly higher IFN responses than dORF3-EGFP, likely due to TRS-CS remodeling. However, it remained unclear whether these changes in viral transcription and replication and in host IFN responses are caused by the TRS-CS remodeling or by the unintended mutations.

To address this, we engineered a series of PEDV mutants by stepwise correction of the unexpected mutations in RMT. To examine whether the effects of the 189-nt insertion are size-

 doi:10.20944/preprints202509.1182.v1

dependent, we also generated a PEDV mutant with a 94-nt insertion, which is half of the 189-nt insertion and contains two 47-nt repeats upstream of E gene TRS-CS. Comprehensive analyses via RNA-seq and real-time reverse transcription-PCR (RT-qPCR) demonstrated that the sgmRNA transcription was significantly altered by the TRS mutations. These changes further impacted viral replication kinetics and host type I and type III IFN responses. While previous studies have engineered recombination-resistant, live-attenuated vaccines (LAVs) by introducing TRS mutations in viruses within the order *Nidovirales* [36–39], this is the first study to systematically quantify how such mutations alter the viral transcription profile and viral replication, and subsequently impact host IFN responses in vitro. Moreover, we demonstrate that a structured insertion in the sequence flanking the TRS-CS can significantly compensate for the transcriptional disruptions caused by TRS-CS remodeling. Our results provide insights into designing recombination-resistant, live attenuated vaccines by TRS remodeling. Beyond PEDV, these findings are broadly relevant to human and animal CoVs and other nidoviruses that rely on TRS-driven transcription.

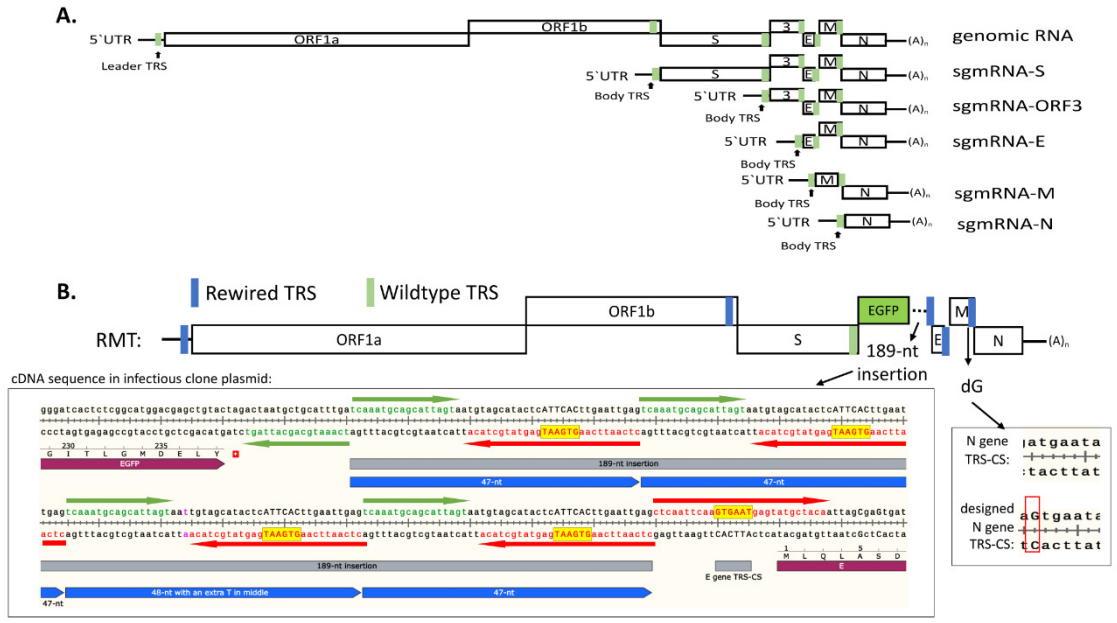

Figure 1. (A) Diagram of PEDV genomic RNA and a set of sgmRNAs generated by discontinuous transcription. Leader TRS and Body TRS are indicated as green bars. (B) The diagram of genome organization of RMT mutant with the location of wild-type (green) and remodeled TRSs (blue). A 189-nt insertion in front of E gene TRS-CS and a missing "G" were detected in RMT mutant. The locations of these two mutations are indicated with black arrows, and the exact double-stranded DNA sequences in the plasmid of our reverse genetic system are shown in the left bottom box. The 189-nt insertion includes three 47-nt and one 48-nt repeats of viral sequences from the primer-pair used for plasmid mutagenesis during TRS-remodeling using reverse genetic system. The reverse and forward primer sequences are indicated with green and red arrows, respectively. The extra "t" in the 48-nt repeat was shown in pink color. The remodeled TRS-CS "GTGAAT" both in positive sense and negative sense are highlighted in yellow. The EGFP and E gene ORFs are indicated by claret arrow bars. The actual N gene TRS-CS sequence and the designed N gene TRS-CS sequence are shown in the right bottom box, with a red box indicating the missing "G".

2. Materials and Methods

2.1. Cells and Reagents

Vero cells (ATCC CCL-81TM) were cultured in Dulbecco's modified Eagle's medium (DMEM, Thermo Fisher Scientific, Waltham, MA, USA) in the presence of 5% fetal bovine serum (FBS, Hyclone, Logan, UT, USA) and antibiotic-antimycotic (100 U/ml penicillin, 100 μg/ml streptomycin,

 doi:10.20944/preprints202509.1182.v1

and 250 ng/ml amphotericin B, Thermo Fisher Scientific). LLC porcine kidney (LLC-PK1) cells (ATCC CL-101) were cultured in modified Eagle's medium (MEM, Thermo Fisher Scientific) supplemented with 5% FBS, 1% nonessential amino acids (NEAA, Thermo Fisher Scientific), 1% antibiotic-antimycotic, and 1% HEPES (Thermo Fisher Scientific). For PEDV propagation, Vero cells were maintained in DMEM supplemented with 0.3% tryptose phosphate broth (TPB, Sigma-Aldrich, St. Louis, MO, USA), antibiotics (100 U/ml penicillin and 100 µg/ml streptomycin, Thermo Fisher Scientific), and 10 µg/ml trypsin (Thermo Fisher Scientific) as described previously [40]. LLC-PK1 cells were maintained in MEM supplemented with 1% antibiotic-antimycotic, 1% NEAA, 1% HEPES, and 10 µg/mL trypsin after the viral inoculation [36,41].

2.2. Generation of PEDV Mutants

The PEDV mutants (Figure 2) were rescued based on the full-length cDNA clone of PEDV strain PC22A as described previously [42]. Briefly, the point mutations were introduced into the plasmid pUC19 carrying the gene fragment of icPC22A (GenBank # KY499262) via NEB Q5® Site-Directed Mutagenesis Kit (NEB, Ipswich, MA). The large piece of gene was inserted or deleted using NEBuilder HiFi DNA Assembly Cloning Kit (NEB). Then the sequence of plasmids was confirmed by Whole Plasmid Sequencing service at Plasmidsaurus (Eugene, OR, USA) using Oxford Nanopore Technology. After digestion of plasmids by restriction enzymes, the appropriately sized cDNA inserts were purified using the QIAquick gel extraction kit (Qiagen, Hilden, Germany). All five fragments (A, B, C, D, and E) were ligated with T4 ligase (NEB) at 4°C overnight in an equal molar ratio for full-length cDNA. The ligated full-length cDNAs were purified by chloroform extraction and used as templates for in vitro transcription using mMessage mMachine T7 transcription kit (Ambion, Austin, CA, USA). The polyadenylated PEDV N gene transcript was generated using HiScribe T7 ARCA mRNA kit (NEB) and co-electroporated into the Vero cells with the full-length transcripts at 450 V and 50 µF using a Gene Pulser II electroporator (Bio-Rad, Hercules, CA, USA). At 6-8 hours after electroporation, the growth medium was discarded, and Vero cells were cultured in maintenance medium in the presence of 10 µg/ml trypsin. Cells were monitored for cytopathic effect (CPE) following infection. In some cases, CPE was not visible within 3 days, requiring a medium change and extended incubation time before harvesting. Once CPE was observed, the virus was harvested and designated as P0 virus. The P0 virus was then subjected to plaque assay, where five individual plaques per virus were initially picked and propagated. The whole genomes of well replicating ones with clear CPE were sequenced by Linear/PCR Sequencing service at Plasmidsaurus. The clone with correct genome sequence was selected for further characterization.

2.3. RNA Secondary Structure Prediction Using mFold

The RNA secondary structure of the 189-nt insertion upstream of the remodeled E gene TRS-CS was predicted using the mFold Web Server [43]. The input sequence was prepared in FASTA format and submitted with default settings for folding temperature (37 °C), ionic conditions (1 M Na+, no Mg2+), and maximum base pairing distance. The output included the minimum free energy (MFE) structure and a set of suboptimal folding ranked by stability.

2.4. Plaque Assay

Monolayers of Vero cells in twelve-well plates were incubated with 10-fold serially diluted PEDV mutants for one hour. After that, the inoculum was removed, and cells were washed with PBS. Then cell monolayers were covered with overlay containing 0.5% agarose in MEM supplemented with 10 µg/ml trypsin and 0.3% TPB [40,44]. At 4 dpi, the cells were fixed with 10% PBS-buffered formalin for 15 minutes and stained with 0.2% crystal violet.

Preprints.org (www.preprints.org) | NOT PEER-REVIEWED | Posted: 15 September 2025 doi:10.20944/preprints202509.1182.v1

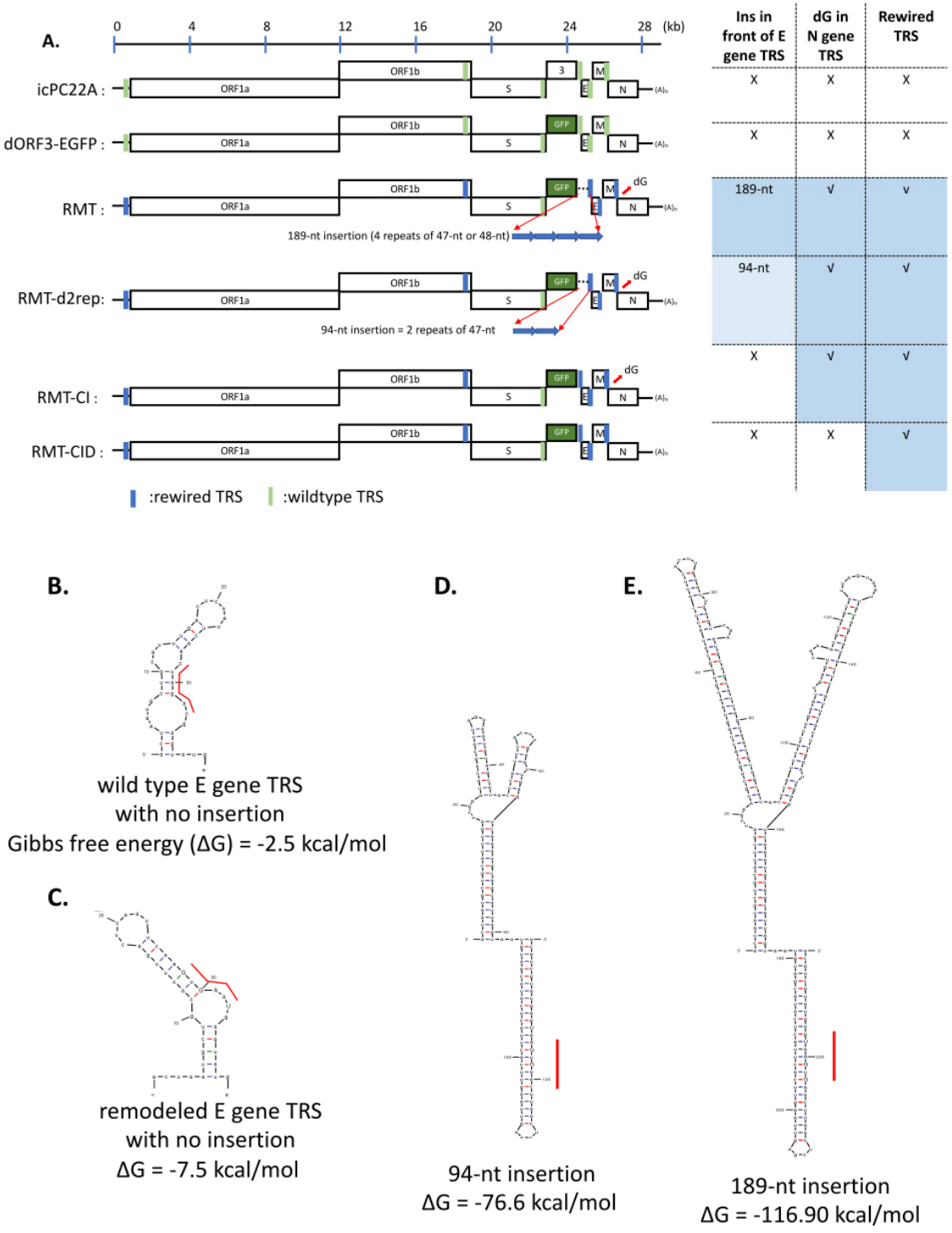

Figure 2. (A) Schematic diagram of the genome organization of infectious clone-derived (ic) PC22A, dORF3-EGFP, RMT, RMT-d2rep, RMT-CI, and RMT-CID. Two unexpected mutations (a 189-nt insertion in front of E gene TRS-CS, and a dG in the TRS-CS of N gene) in the RMT mutant are indicated by red arrows. The table on the right summarizes the mutations harbored in each mutant, with "x" for absent and "√" for present. The predicted secondary structures for the (B) wild-type TRS region of E gene, and the remodeled TRS region of E gene with (C) no insertion, (D) 94-nt insertion, and (E) 189-nt insertion. The TRS-CSs are marked by red lines. Gibbs free energy for each structure is presented.

 doi:10.20944/preprints202509.1182.v1

2.5. Growth Kinetics for PEDV Mutants

Vero or LLC-PK1 cell monolayers in twelve-well plates were infected with the corresponding viruses at a MOI of 0.01. After the one-hour adsorption, cell monolayers were washed with PBS (-) to remove those unbound virions and cultured in maintenance medium. Both cells and supernatants were collected at multiple time points and titrated in 96-well plates for 50% tissue culture infective doses ($TCID_{50}$) by the Reed-Muench method [45].

2.6. The Detection of PEDV Genomic and sgmRNA by Reverse Transcription-Quantitative PCR (RT-qPCR)

For the detection of genomic RNA and sgmRNA, Vero cells or LLC-PK1 cells were inoculated with individual PEDV mutants at a MOI of 1. After the 1 h adsorption, the virus inoculum was removed, and the cells were washed with PBS (-). At the indicated hpi, supernatants were discarded, and total cellular RNA was extracted with TRIzol reagent (Thermo Fisher Scientific). Genomic RNA levels were determined by one-step RT-qPCR using the OneStep RT-PCR kit (Qiagen) with forward and reverse primers and a probe targeting nsp1 gene (Table 1). All the sgmRNA levels were determined by two-step RT-qPCR using the same OneStep RT-PCR kit but only adding reverse primer during reverse transcription, then adding forward primer and probe for PCR. Copy numbers of each amplicon were determined by standard curves. Relative sgmRNAs level were expressed as the ratio of sgmRNA to gRNA.

Table 1. RT and qPCR primer and probe sequences for PEDV genomic RNA and sgmRNA detection.

Target	Forward primers (5′-3′)	Reverse primers (5′-3′)	Probes (5′-3′)
gRNA (nsp1)	TGAAGCCGTCTCATACTATTCTG	AATCCCTCAACAGTGTCAGC	FAM-TGCAATGCCGTTTCGTGTCCTTC-BHQ
sgmRNA-S	CTATCTACGGATAGTTAGCTC	GAACCGCCTAAAATTAGTGT	FAM-CCACAAGATGTCACCAGGTGCTCAGCT -IBFQ
sgmRNA-E	CTATCTACGGATAGTTAGCTC	AGGTGTGTAAACTGCGCTATTA	FAM-TCTGTGCTTCACTTGTCACCGGTTGT-IBFQ
sgmRNA-M	CTATCTACGGATAGTTAGCTC	TATCGTCAGTATGATATTCCATG	FAM-ATTCAAGTGAATGAAATATGTCTAACGG -IBFQ
sgmRNA-N	CTCTTGTCTACTCAATTCAACTAAACAGAAAC	CCAGTATCCAATTTGCTGGTCC	FAM-TCAGGATCGTGGCCGCAAAC-BHQ

2.7. The Detection of PEDV RNA Junction by RNA-seq

RNA-seq was performed by CD Genomics (Shirley, NY, USA). The cDNA library was prepared from total RNA extracted from the PEDV mutant infected Vero cells following ribosome RNA depletion. A target amount of 100 million 150 base pair paired-end reads per sample was sequenced on an Illumina NovaSeq 6000. Raw reads were trimmed using Trim Galore version 0.6.10 (https://github.com/FelixKrueger/TrimGalore) with option --trim-n and otherwise with default parameters. Trimmed reads were pooled and aligned to the reference genome of the corresponding PEDV mutant using ViReMa version 0.25 [46] with options: -BED --Pad 200 --MicroInDel_Length 5 --Defuzz 0 -FuzzEntry and otherwise with default parameters.

 doi:10.20944/preprints202509.1182.v1

2.8. Interferon Induction Assay

The LLC-PK1 cells were inoculated with individual PEDV mutants at an MOI of 1. After the 1 h adsorption, the virus inoculum was removed, and the cells were washed with PBS (-). At 12 hpi, the supernatants were collected to titrate viral infectious titer by $TCID_{50}$, and the total cellular RNA was extracted with TRIzol reagent (Thermo Fisher Scientific). Then, cellular DNA was removed by treating with DNase I (Qiagen). Viral total N gene RNA levels were determined by PEDV-specific reverse transcription-quantitative PCR (RT-qPCR) using the OneStep RT-PCR kit (Qiagen) with forward and reverse primers (forward, 5`-CGCAAAGACTGAACCCACTAAC-3`; reverse, 5`-TTGCCTCTGTTGTTACTTGGAGAT-3`) and a probe (5`-FAM-TGYYACCAYYACCACGACTCCTGC-BHQ-3`) [42]. The copy number was determined by standard curves. One microgram of total RNA was reverse transcribed using SuperScript™ IV Reverse Transcriptase and random hexamers (Thermo Fisher Scientific). The cDNA was subjected to quantitative PCR using SYBR green PCR mix (Thermo Fisher Scientific) according to the manufacturer's instructions. Primers for IFN detection were described previously [47]. The β-actin gene was used as an internal control. The threshold cycle (CT) values for target genes and the differences in their CT values (ΔCT) were determined. Relative transcription levels of target genes are presented as fold changes relative to the mock controls using the $2^{-\Delta\Delta CT}$ threshold method [48].

2.9. Statistical Analysis

The statistical analyses were performed using GraphPad Prism 10.3. Data in Figures 3, 4, 6, and 7 are shown in Mean ± standard deviation (SD) and analyzed by one-way analysis of variance (ANOVA) followed by Tukey's multiple-comparison test. Groups with significant difference ($P < 0.05$) were indicated with different letters.

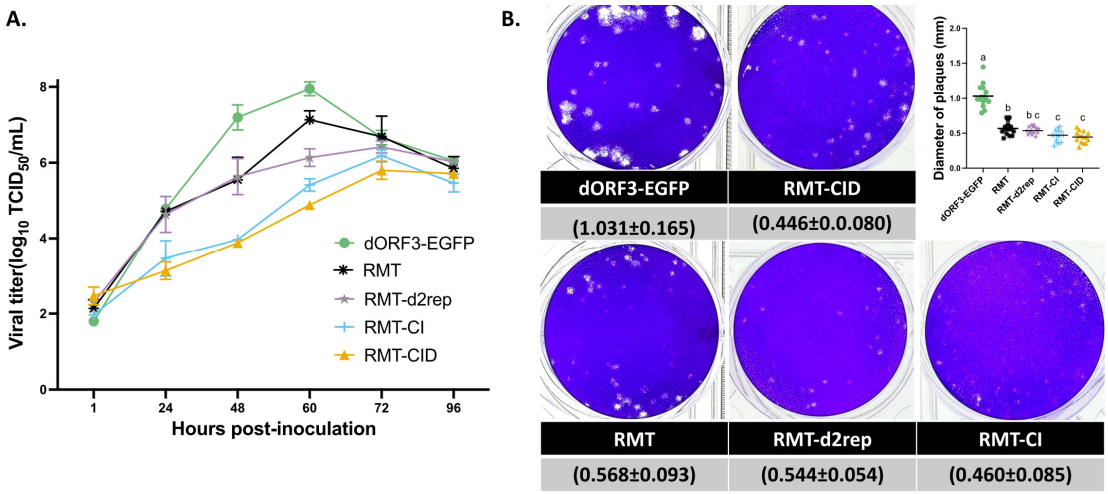

Figure 3. Characterization of the infectious clone-derived PEDV mutants' replication in Vero cells. (A) Multi-step growth kinetics of the PEDV mutants in Vero cells infected with the individual virus at a multiplicity of infection of 0.01. (B) Plaques of recombinant PEDV mutants in Vero cells with 0.5% final concentration of agarose overlay. The cells were fixed and stained at 4 days post-inoculation. The inset shows the diameters of 15 plaques, with the mean shown as a line. Results are presented as mean ± SD in the table. Groups with significant differences ($p < 0.05$) are indicated with different letters.

 doi:10.20944/preprints202509.1182.v1

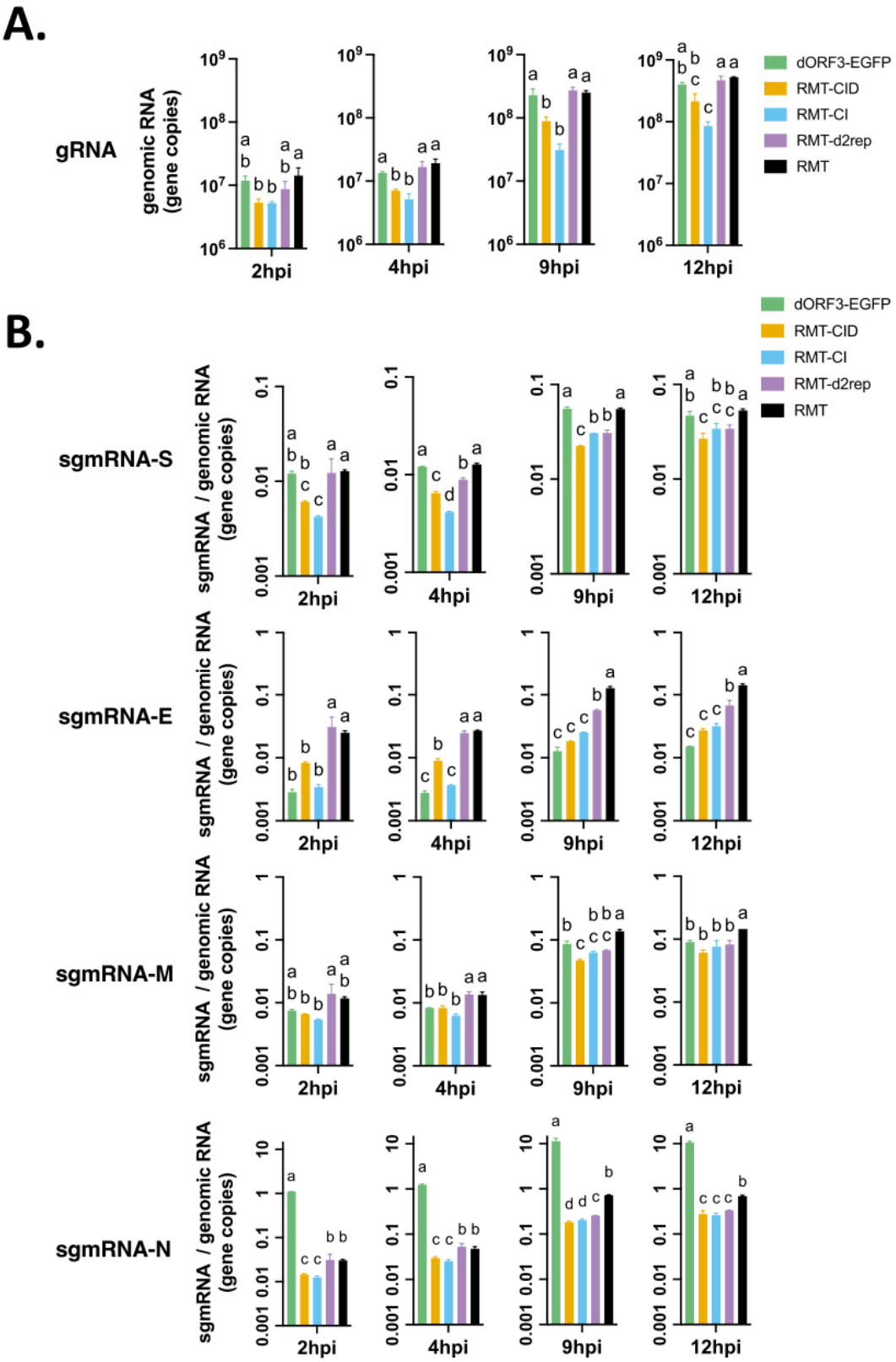

Figure 4. Relative sgmRNA abundance analysis of PEDV mutants in Vero cells using RT-qPCR. (A) Genomic RNA gene copies and (B) sgmRNA-S, sgmRNA-E, sgmRNA-M, and sgmRNA-N were normalized to genomic RNA levels at early (2 and 4 hpi) and late (9 and 12 hpi) time points of one cycle of virus replication. Results are presented as mean ± SD. Groups with significant differences ($p < 0.05$) are indicated with different letters.

 doi:10.20944/preprints202509.1182.v1

3. Results

3.1. A Series of PEDV Mutants Were Rescued Using Reverse Genetics

We identified two unexpected mutations in the TRS regions of the RMT mutant [36], including an 189-nt insertion upstream of E gene TRS-CS and a missing "G" in the N gene TRS-CS. The 189-nt insertion includes three 47-nt and one 48-nt tandem repeats of viral sequences (Figure 1B), originating from the primer-pair used during plasmid mutagenesis for TRS-remodeling in our reverse genetics system [21]. In this system, the full-length PEDV genome cDNA is assembled from five plasmids and transcribed in vitro to generate viral genomic RNA for transfection into Vero cells and subsequent virus rescue. The site-directed plasmid mutagenesis used for TRS remodeling involved PCR amplification from the plasmid for assembling dORF3-EGFP, phosphorylation, ligation, and plasmid amplification in *E. coli*. The 189-nt insertion, which consists of repeated sequences derived from PCR primers used in the mutagenesis process, was detected in both the mutated plasmid and the rescued RMT virus. However, the precise mechanism underlying this insertion remains unknow and is beyond the scope of this study.

To further investigate the effects of these mutations, we designed and rescued three more mutant viruses in addition to the previously reported two mutants, using reverse genetics of PEDV PC22A strain (Figure 2A). The icPC22A was the infectious clone-derived highly virulent PEDV PC22A strain with intact ORFs and wild-type TRS [21]. The dORF3-EGFP was generated by replacing the ORF3 with EGFP and was a reporter virus [36]. The RMT was constructed from dORF3-EGFP by remodeling all TRS-CS except for the one in front of EGFP and carries both the 189-nt insertion and "G" deletion [36]. The RMT-d2rep was created from RMT by deleting two of the four tandem repeats and has 94-nt insertion. The RMT-CI was the "corrected insertion" version of RMT. Finally, RMT-CID was the "corrected insertion and deletion" version of RMT. The RNA secondary structure prediction demonstrated significant structural changes due to the insertions (Figure 2B–E). The remodeled TRS-CS with the surrounding sequences in front of the E gene was predicted to have low stability (ΔG = -7.5 kcal/mol, Figure 2C), similar to wild-type E gene TRS-CS (ΔG = -2.5 kcal/mol, Figure 2B). However, the 94-nt and 189-nt insertions notably increased structural complexity, resulting in moderate (ΔG = -76.6 kcal/mol, Figure 2D) and high stability (ΔG = -116.9 kcal/mol, Figure 2E), respectively. These structural changes likely interfere with viral transcription.

3.2. The Mutations in the TRS Region Changed PEDV Replication Kinetics and Plaque Morphology in Vero Cells

To determine the impact of these TRS mutations on viral replication, multi-step growth kinetics of the PEDV mutants were performed in Vero cells with a multiplicity of infection (MOI) = 0.01 (Figure 3A). RMT-d2rep, RMT-CI and RMT-CID reached the peak infectious titers at 72 hours post-inoculation (hpi), which were slower than RMT and dORF3-EGFP (60 hpi). In addition, RMT-CID replicated to a lower peak infectious titer (5.80 ± 0.24 $TCID_{50}$/mL) than dORF3-EGFP (7.95±0.18 $TCID_{50}$/mL), indicating that remodeling the TRS-CS suppressed viral replication. RMT-CI and RMT-CID replicated to similar peak infectious titers, indicating that the "G" deletion in N gene TRS-CS had no obvious impact on viral replication. Moreover, the RMT replicated to a higher peak infectious titer (7.1 ± 0.23 $TCID_{50}$/mL) than RMT-d2rep (6.42 ± 0.16 $TCID_{50}$/mL) and RMT-CI (6.18 ± 0.16 $TCID_{50}$/mL), indicating that the 189-nt insertion partially compensated the suppressive effects on viral replication of the remodeled TRS-CS but the 94-nt insertion did not. Interestingly, RMT-d2rep replicated as efficiently as RMT before 48 hpi, but its replication efficiency was subsequently reduced for unknown reasons.

Correspondingly, plaque assays revealed significant differences in plaque sizes among the mutants (Figure 3B). dORF3-EGFP produced the largest plaques (1.031 ± 0.165 mm in diameter), whereas RMT, RMT-d2rep, RMT-CI, and RMT-CID formed significantly smaller plaques. RMT-CID (0.446 ± 0.080 mm) and RMT-CI (0.460 ± 0.085 mm) had the smallest plaques with no significant difference between them. RMT produced significantly larger plaques (0.568 ± 0.093 mm) than RMT-

 doi:10.20944/preprints202509.1182.v1

CID and RMT-CI. The plaque size of RMT-d2rep (0.544 ± 0.054 mm) was between those of RMT and RMT-CI, without statistical differences. These findings indicate that the remodeled TRS-CS suppressed viral replication and cell-to-cell spread in Vero cells. The 189-nt insertion in the TRS flanking region partially compensated this negative impact, while the 94-nt insertion and "G" deletion did not.

3.3. TRS Mutations Disrupted the Subgenomic RNA Transcription of PEDV in Vero Cells

TRS is essential for CoV discontinuous transcription, which generates a nested set of sgmRNAs. Previously, an unusual transcriptional profile of RMT was observed, in which sgmRNA-E surpassed sgmRNA-N in abundance, deviating from the canonical hierarchy observed in PEDV carrying wild-type TRS (dORF3-EGFP) [36]. To further investigate how TRS mutations in RMT affect PEDV transcription, we quantified the genomic RNA and the relative levels of four structural protein gene sgmRNAs (sgmRNA/gRNA) in Vero cells infected with equal MOI of 1 at early (2 hpi and 4 hpi) and late (9 hpi and 12 hpi) stages of one viral replication cycle using RT-qPCR (Figure 4). At both early and late time points, similar trends were observed where dORF3-EGFP, RMT and RMT-d2rep showed the highest gRNA levels, while RMT-CID and RMT-CI showed reduced gRNA accumulation, consistent with their impaired replication phenotypes.

The relative sgmRNA abundance showed intriguing patterns (Figure 4B). Compared with dORF3-EGFP, RMT-CID had significantly lower levels of sgmRNA-S and sgmRNA-N, but similar levels of sgmRNA-M and sgmRNA-E, at both early and late time points. These results were caused by the remodeled TRS-CS in RMT-CID and in agreement with its impaired replication and smaller plaques (Figure 3), since the N protein is essential for viral gene replication [24,49–51] and the S protein is involved in cell-to-cell spread [40,52,53]. RMT-CI and RMT-CID showed generally similar sgmRNA profiles, with a few exceptions, indicating that the "G" deletion in the N gene TRS-CS had minimal impact on transcription and replication. Among RMT, RMT-d2rep and RMT-CI, at late time point 12 hpi, RMT had the highest level of sgmRNAs for all the four structural proteins, while RMT-d2rep only significantly increased the sgmRNA-E level compared with RMT-CI. These results suggest that the 189-nt insertion significantly enhanced the transcription of all four structural protein sgmRNAs, while the shorter 94-nt insertion (RMT-2rep) selectively enhanced only sgmRNA-E, resulting in an insertion-size-dependent effect on sgmRNA-E levels. Interestingly, at early time points (2 hpi and 4 hpi), RMT and RMT-d2rep both showed significantly elevated levels of sgmRNA-S, -E, -M, and -N compared with RMT-CI, suggesting that the 94-nt insertion can also enhance early-stage overall structural protein sgmRNA transcription like the 189-nt insertion. However, only the 189-nt insertion (RMT) maintained enhanced transcription throughout the infection cycle. This early but transient transcriptional boost by the 94-nt insertion may explain RMT-2rep initial replication kinetics being similar to RMT (Figure 3A), despite lower replication efficiency at later stages. Together, these findings demonstrate that TRS-CS remodeling disrupted the PEDV sgmRNA transcription profile, while the 189-nt insertion in front of E gene TRS-CS acts as a compensatory enhancer of sgmRNA transcription in an insertion size-dependent manner.

3.4. Canonical and Non-Canonical sgmRNA Syntheses Were Altered in TRS Mutants in Vero Cells

To comprehensively characterize both canonical structural protein sgmRNAs and non-canonical transcriptional products of PEDV, we performed RNA-seq on Vero cells infected with dORF3-EGFP, RMT-CID, RMT-CI, or RMT and harvested at 8 hpi. RNA-seq analysis provided deeper insights into the transcriptional accuracy change due to TRS-CS remodeling. Junction-spanning reads corresponding to template switch events were identified and mapped to the viral genome (Figure 5A) [46]. These included canonical sgmRNAs derived from the template switching of each structural protein genes' TRS-B to TRS-L, as well as diverse non-canonical junctions likely resulting from aberrant template switching.

Quantification of canonical sgmRNA junctions revealed distinct transcriptional profiles among the mutants (Figure 5B). dORF3-EGFP exhibited the highest and lowest proportion of canonical

 doi:10.20944/preprints202509.1182.v1

sgmRNAs and other defective viral RNA reads (68.988% and 31.012%, respectively, of total viral RNA reads), consistent with its robust TRS-dependent transcription. In contrast, RMT-CID and RMT-CI showed markedly reduced levels of canonical sgmRNAs and an increased proportion of defective viral RNA (64.292% and 71.596%, respectively), indicating impaired discontinuous transcription accuracy. RMT maintained intermediate levels of canonical sgmRNAs (51.121%), with notably elevated sgmRNA-E frequency (14.868%), further supporting the compensatory effects of the 189-nt insertion upstream of the E gene TRS-CS.

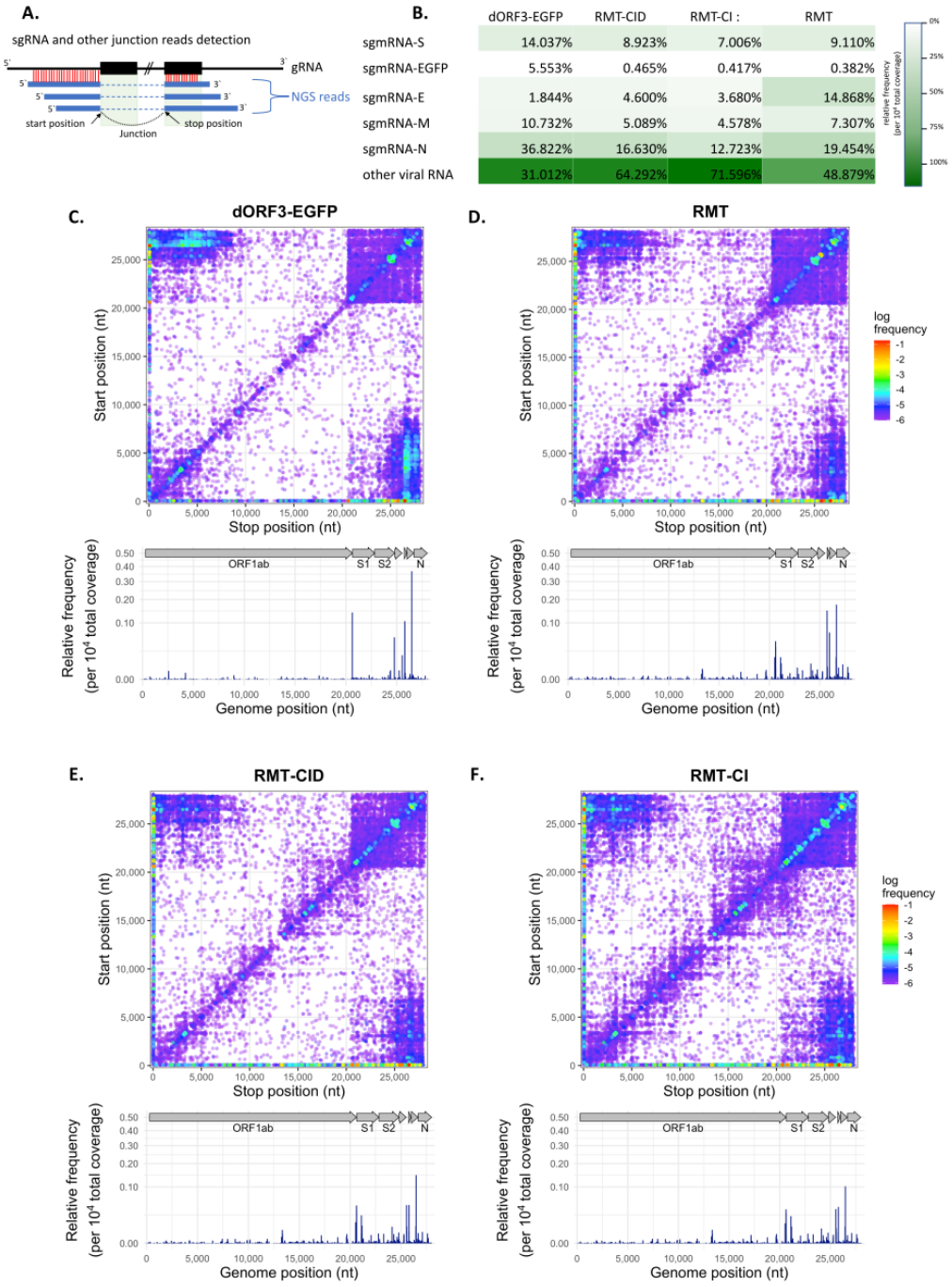

Figure 5. Mapping of template switches in the dORF3-EGFP-, RMT-CID-, RMT-CI- or RMT-infected Vero cells. (A) Schematic of the strategy used to detect junction reads with RNA sequencing. The NGS reads are represented as blue bars, and the template switches are represented by curved dashed lines and identified by junctions in NGS reads. The start position and stop position of template switch are indicated with a black arrow. (B) Relative frequencies of canonical sgmRNAs and other viral RNAs detected in cells infected with each PEDV mutant. Frequencies are shown as the percentage of total viral RNA reads. Darker green indicates higher frequency;

 doi:10.20944/preprints202509.1182.v1

white indicates the lowest detected levels. (C-F) Intra-genomic template switch junctions are mapped according to their genomic position and colored according to their log-scaled frequency in the population of all junctions in the cells infected with dORF3-EGFP (C), RMT (D), RMT-CID (E) or RMT-CI (F). The highest frequency junctions are red and completely opaque. The lowest frequency junctions are blue and the most transparent. Lower panels show the distribution of junction stop positions for junctions initiating from the leader TRS (TRS-L), plotted as relative frequency of total viral RNA reads. Annotated viral ORFs are shown for reference.

Genome-wide mapping of junctions revealed broad changes in template switching activity across the mutants (Figure 5C–F). In dORF3-EGFP-infected cells, junctions were concentrated at canonical TRS-CS positions, whereas in RMT-CID and RMT-CI, non-canonical junctions were dispersed throughout the genome (upper panels), with increased frequency at internal genomic sites. The different genome positions jumping to TRS-L junction frequency plots (lower panels) confirmed that dORF3-EGFP produced a typical sgmRNA hierarchy dominated by sgmRNA-N and lowest in sgmRNA-E, while mutants with remodeled TRS-CS showed disrupted transcription profiles with reduced level of canonical sgmRNAs but "noisier" non-canonical sgmRNAs. Notably, although RMT also had an inaccurate template switch due to the remodeled TRS-CS with "noisy" non-canonical sgmRNAs, the ratio of canonic sgmRNAs abundance were higher than RMT-CI, due to the 189-nt insertion.

Taken together, these data demonstrate that remodeling the TRS-CS impairs canonical template switching and increases transcriptional "noise", while the 189-nt insertion in RMT increased canonical sgmRNA levels and partially restored the transcription accuracy, emphasizing the complex interplay between leader and body TRS-CS base pairing and the structure of TRS flanking sequences on RNA transcription accuracy and viral fitness.

3.5. Effects of TRS Mutations on Type I and Type III IFN Responses, Viral Replication and sgmRNA Abundance in Porcine LLC-PK1 Cells

We further investigated how the TRS mutation-induced inaccurate transcription influences host immune responses in porcine LLC-PK1 cells (Figures 6 and 7). First, we examined the replication efficiency and sgmRNA abundance of the PEDV mutants in LLC-PK1 cells. Viral growth kinetics (Figure 6A) demonstrated the same replication patterns of the mutants to those in Vero cells, with dORF3-EGFP reaching the highest peak infectious titer at 48 hpi (6.05 ± 0.35 $TCID_{50}$/mL), indicating the highest replication efficiency. RMT-CID (4.72 ± 0.12 $TCID_{50}$/mL) and the RMT-CI (4.58 ± 0.07 $TCID_{50}$/mL) reached lower peak titers at 72 hpi, displaying most reduced viral replication efficiency. The RMT (5.14 ± 0.23 $TCID_{50}$/mL) reached higher peak infectious titer at 48 hpi that was earlier than RMT-CID and RMT-CI. Interestingly, the RMT-d2rep (4.47 ± 0.23 $TCID_{50}$/mL) replicated similarly to RMT at early stage but less efficiently at later stages, particularly after 36 hpi.

Further, quantification of gRNA and sgmRNA abundance using RT-qPCR in LLC-PK1 cells, which is an IFN-sufficient cell line (Figure 6), revealed results comparable to those observed in Vero cells (Figure 4). The gRNA level (Figure 6B) at 12 hpi was consistent with the replication efficiency observed in growth kinetics (within 24 hpi), following the trend: dORF3-EGFP > RMT and RMT-d2rep > RMT-CI and RMT-CID. The sgmRNA-E gene level was significantly elevated following TRS-CS remodeling, as demonstrated by the comparison between RMT-CID and dORF3-EGFP (Figure 6D). As expected, sgmRNA-E levels followed the trend of RMT > RMT-d2rep > RMT-CID and RMT-CI, correlating with the size of the insertions upstream of the E gene TRS-CS. The most dramatic reduction was observed for sgmRNA-N transcripts (Figure 6F). The sgmRNA-N levels were most reduced in the RMT-CID, RMT-CI, and RMT-d2rep mutants, followed by RMT, when compared to the parental dORF3-EGFP. This suggests that the 189-nt insertion in RMT partially compensates for the reduction. Unlike the significant differences observed in Vero cells, the sgmRNA-S levels in RMT-infected cells were slightly but not significantly higher than the others (Figure 6C). The RMT had significantly higher sgmRNA-M level than RMT-d2rep and RMT-CI, due to the 189-nt insertion (Figure 6E).

 doi:10.20944/preprints202509.1182.v1

The RMT-CID mutants induced significantly higher IFN-β and IFN-λ1 responses in the LLC-PK1 cells than the parental dORF3-EGFP mutant, due to the remodeled TRS-CS (Figure 7A,B). The RMT-CI, RMT-d2rep and RMT-CID induced similarly high levels of IFNs, suggesting the missing "G" or the 94-nt insertion did not affect the IFN responses. Compared with RMT-CI, the RMT induced significantly lower levels of IFNs, which were still slightly higher than the parental dORF3-EGFP mutant with no significant difference. Additionally, PEDV total RNA shedding targeting N gene (including all genomic and sgRNA) and infectious titer were significantly lower in RMT-CID compared to that in dORF3-EGFP at 12 hpi, while both RNA and infectious titers of RMT were similar to dORF3-EGFP (Figure 7C,D). These data suggest that remodeling the TRS-CS enhanced innate immune responses, and that the 189-nt insertion may counteract this effect by increasing sgmRNA level and reducing the proportion of defective viral RNA.

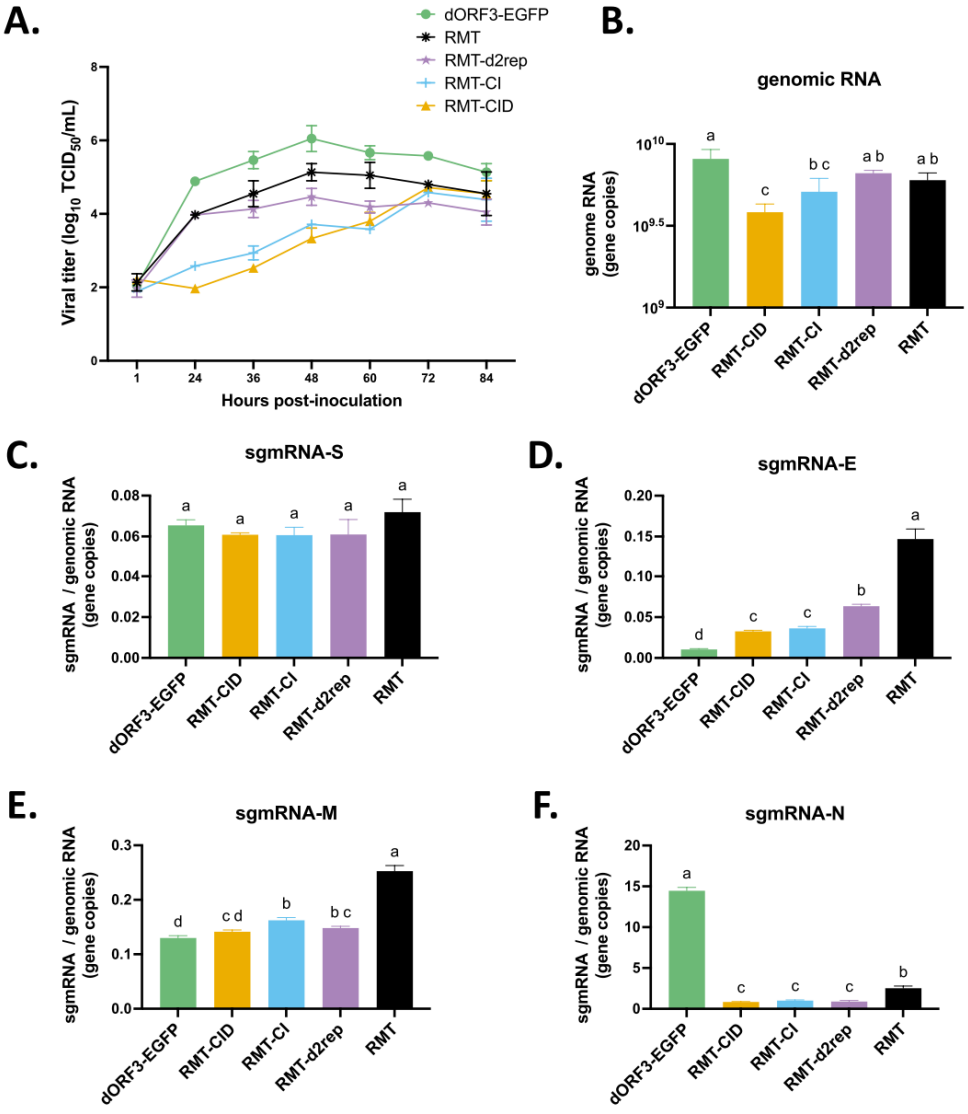

Figure 6. Viral replication kinetics and sgmRNA abundance of PEDV mutants in LLC-PK1 cells. (A) Multi-step growth kinetics of PEDV mutants in LLC-PK1 cells. Cells were infected at MOI = 0.01, and viral titers were quantified at the indicated time points by TCID50 assay. (B-F) Quantification of genomic RNA and individual sgmRNAs in infected LLC-PK1 cells at 12 hpi. Total RNA was extracted and analyzed by RT-qPCR. Genomic RNA is presented as copies per μg total RNA (B), and sgmRNA-S (C), sgmRNA-E (D), sgmRNA-M (E), and sgmRNA-N (F) abundance is shown as the ratio of sgmRNA to genomic RNA copies. Data represent mean ± SD. Groups with significant differences ($p < 0.05$) are indicated with different letters.

 doi:10.20944/preprints202509.1182.v1

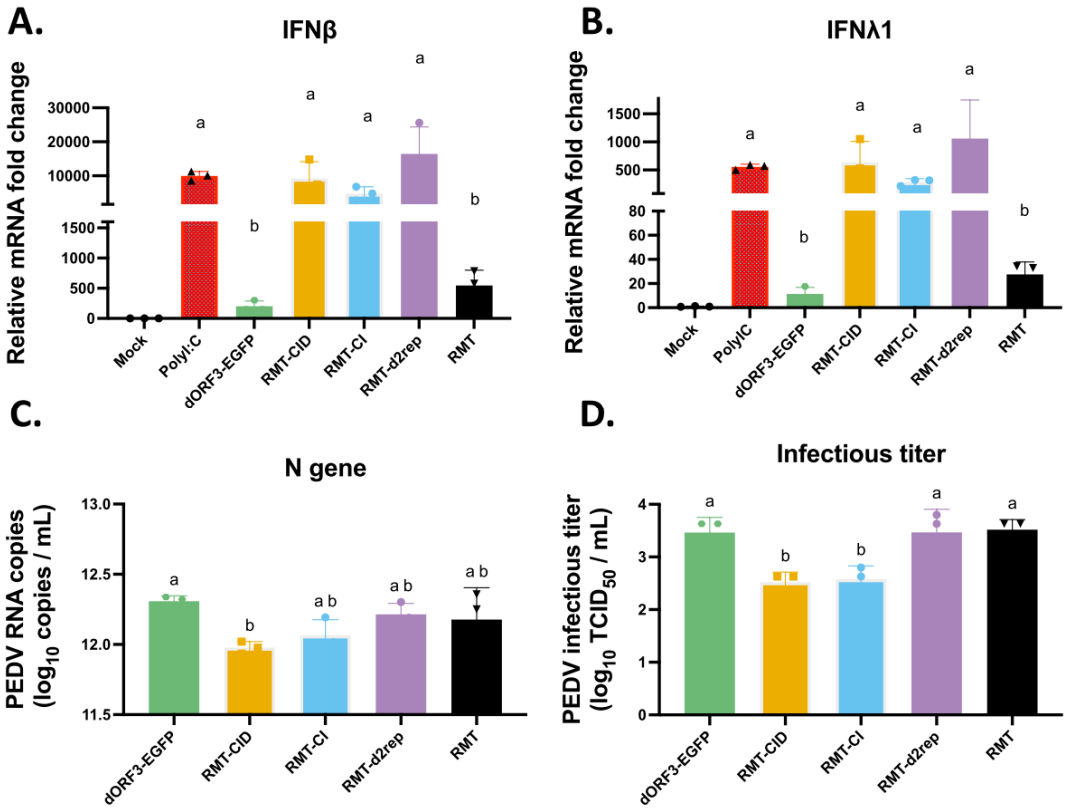

Figure 7. Induction of type I and type III IFN mRNAs by the PEDV mutants in LLC-PK1 cells. The cells were inoculated with each virus at a MOI of 1 or medium (mock) or stimulated with poly I:C as a positive control. At 12 hpi, the supernatants were collected for testing viral infectious titers, and cells were lysed for measuring IFN mRNA levels, including IFN-β (A) and IFN-λ1 (B). The PEDV total N gene RNA levels (C), and viral infectious titers in TCID50 (D) are shown. Groups with significant differences ($p < 0.05$) were indicated with different letters.

4. Discussion

CoVs transcribe a nested set of sgmRNAs through a discontinuous transcription mechanism regulated by TRSs. In this study, we dissected how the engineered mutations in the TRS region of PEDV—including the remodeled TRS-CS, a 189-nt insertion upstream of E gene TRS-CS, and a guanine deletion within N gene TRS-CS—modulate viral transcription, replication efficiency, and host innate IFN responses. Our findings highlight that the architecture of TRS regions—beyond core sequence identity—also plays an important role in governing template-switching events during CoVs transcription. This expands our understanding of the fundamental mechanisms of CoV gene transcription regulation and may have broader relevance to other viruses in the order of Nidovirales that also use TRS-mediated discontinuous transcription, such as porcine reproductive and respiratory syndrome virus (PRRSV) in Arteriviridae [20,38]. It also informs rational strategies for development of attenuated CoV vaccines [36,37,39,54,55].

TRS-CS is a concept identified in CoVs, referring to a conserved nucleotide motif located upstream of each ORF which shares the highest sequence complementarity with the leader TRS-CS. This complementarity facilitates accurate template switching during the synthesis of (-) sgRNAs, ensuring that only the minimal necessary amount of (-) sgRNA intermediates is produced. These limited (-)sgRNA templates support efficient synthesis of abundant sgmRNAs for each ORF, making the process streamlined and resource-efficient for viral replication. Additionally, because the resulting capped (+) sgmRNAs resemble host mRNAs, they are more likely to evade detection by innate immune sensors. Limiting the production of (-) sgRNA also helps reduce the risk of triggering

 doi:10.20944/preprints202509.1182.v1

host immune responses. Consequently, in nature, the most efficient and exclusive TRS-CS combinations are positively selected, outcompeting less optimal variants. However, when we remodeled the PEDV TRS-CS to "GTGAAT", this finely tuned balance was disrupted. The remodeled TRS-CS cannot competitively block other pairing events, weakening its ability to dominate template switching and resulting in the accumulation of aberrant non-canonical transcripts.

In CoVs, the leader TRS-CS is conserved within genera but varies between genera, with the exception of *Embecoviruses* where the leader TRS-CS is similar to *Alphacoronavirus* [56]. The body TRS-CS is typically identical to the leader TRS-CS within a given genome or differs by only one nucleotide in most CoVs, including SARS-CoV-2, SARS-CoV, MERS-CoV, Swine Acute Diarrhea Syndrome Coronavirus (SADS-CoV), and HCoV-HKU1 [56]. However, in PEDV, the body TRS-CS can differ by more than two nucleotides from the leader TRS-CS [36], a unique feature whose evolutionary significance remains unclear. One hypothesis is that the greater TRS-CS diversity in PEDV may enhance its potential to recombine with CoVs from other genera, thereby facilitating gene exchange and accelerating viral evolution. For example, a novel swine enteric coronavirus resulting from recombination of PEDV in *Pedacovirus* and transmissible gastroenteritis virus (TGEV) in *Tegacovirus* has been identified [57].

Although the TRS-CS for canonical sgmRNAs is generally conserved and rarely mutated in CoVs, the emergence of novel TRS-CS motifs has been observed during SARS-CoV-2 evolution. For example, a novel TRS-CS in the B.1.1 lineage of SARS-CoV-2 enabled the expression of a truncated C-terminal N protein, which functioned as a type I IFN antagonist and enhanced viral replication in vitro [58,59]. Moreover, researchers successfully rescued a reporter HCoV-OC43 virus by inserting an artificial TRS sequence identical to the N gene TRS-CS and its flanking sequence (GAAAUAAUAUCUAAAUUUUAAGG) upstream of a reporter gene ORF, enabling production of the reporter protein from a novel sgmRNA without disrupting the viral transcription and replication [60]. These examples highlight how natural evolution and artificial manipulation of TRS-CSs can modify sgmRNA expression and viral behavior.

In our study, remodeling TRS-CSs across PEDV genome significantly impaired canonical sgmRNA production, reduced replication efficiency in Vero and LLC-PK1 cells, and increased IFN-β and IFN-λ1 induction. RNA-seq analysis revealed widespread transcriptional "noise" in these mutants, with an elevated proportion of non-canonical transcripts and reduced canonical junctions. These data confirm that even perfectly matched TRS-CSs, when placed into a foreign sequence context, disrupt template switching accuracy, suggesting that both flanking sequence composition around TRS-CS and local RNA secondary structure are determinants for template switching associated with viral sgmRNA transcription. This is further supported by our observation that the single nucleotide mismatch caused by "G" deletion in N gene TRS-CS did not affect sgmRNA-N gene abundance. Additionally, when generating the RMT mutant, we introduced a silent mutation to modify a pre-existing "GTGAAT" sequence within the E gene ORF (naturally present in the wild-type PEDV genome) to "GCGAGT" to prevent unintended template switching within the E gene [36]. However, RNA-seq data in this study demonstrated that it did not abolish template switching at that locus (Table S1). In addition, the set of TRS-CS in wild-type PEDV is not identical but still conducts very accurate TRS-B to TRS-L template switch. Overall, these data suggest that partial mismatches within the TRS-CS do not necessarily prevent TRS-B and TRS-L template switching and that the surrounding sequences or RNA structure may contribute significantly to TRS recognition. This tolerance for TRS-CS mismatch might explains the transcriptional "noise" in PEDV mutants carrying the remodeled TRS-CS. Although there is no identical "GTGAAT" in the PEDV genome besides the remodeled TRS-CSs, we cannot prevent the pairing at sequences with one- or two-nucleotide-mismatch. Furthermore, base-pairing involves more than just the strongest A-U and G-C Watson-Crick interactions. G-U wobble pairs are common in RNA, and U-U has also been observed [61]. In addition, template switching efficiency should not be assessed solely based on the 6–8-nucleotide conserved TRS-CS but should also consider the overall binding efficiency across flanking sequence surrounding the leader and body TRS-CSs. A recent study of HCoV-OC43 [62] analyzed sequence

 doi:10.20944/preprints202509.1182.v1

similarity between 20-nt regions of TRS-B and TRS-L including flanking sites beyond the most conserved TRS-CS "AUCUAAAC" in *Embecovirus [56],* and revealed that non-canonical transcripts generally had weaker similarity between their TRS-B and TRS-L than canonical sgmRNAs, consistent with their lower abundance. Notably, there were exceptions: the TRS-B of HE gene showed less similarity to TRS-L than some non-canonical TRS-B sites, indicating that factors beyond simple sequence similarity influence template switching efficiency. These observations underscore the importance of flanking sequences and structural elements, setting the stage for our analysis of how flanking sequence insertions modulate discontinuous transcription. Modification of RNA structure surrounding TRS-L has been reported to affect its binding with TRS-B and impact viral replication in TGEV [63], and the 189-nt insertion in this study supported that significant alteration of the RNA structure surrounding TRS-B can influence viral fitness.

This 189-nt insertion partially restored canonical sgmRNA synthesis, improved viral replication and counteracted the enhanced IFN responses due to reduced accuracy in discontinuous transcription. The repetitive sequence of the 189-nt insertion forms a large and stable secondary structure that acts as an "obstacle" to the replicase complex during its transcription of the PEDV genome. It potentially causes the replicase complex to pause and increases the frequency of template switching to the TRS-L. The sgmRNA accumulation due to complex RNA secondary structure upstream of TRS is not limited to CoVs. A recent study of PRRSV [64] demonstrated that a stable RNA secondary structure upstream of N gene TRS significantly enhanced not only downstream sgmRNA-7, but also upstream sgmRNA-2 and -6 accumulation and promoted viral replication, further supporting the broader role of RNA structures in *Nidovirus* transcriptional regulation. In addition, the 189-nt insertion includes four reverse complementary sequences of the TRS-CS motif "ATTCAC", which may promote long-distance RNA-RNA interactions, increase the proximity or accessibility of TRS-L to the 3′-end of the genome, and further enhance its base-pairing with all TRS-Bs. Similar findings were reported for SARS-CoV-2 [65,66], where long-distance RNA-RNA interactions involving the 5′ and 3′ UTRs regulate template switching. The 189-nt insertion may mimic such long-distance base-pairing and enhance all canonical sgmRNA transcription in PEDV. In TGEV, similar long-distance RNA-RNA interactions pulled TRS-B and TRS-L into proximity and further enhanced sgmRNA transcription [28]. Moreover, tandem repeat sequence has been reported as gene expression enhancer in DNA virus. In duck circovirus, a unique quadruple tandem repeat sequence between its *rep* and *cap* genes enhanced the viral mRNA stability and increased viral gene expression [67]. Interestingly, the enhancement of sgmRNA-E transcription appears to be size- or structure-dependent, with the strongest effect observed in RMT, followed by RMT-d2rep (moderate) and RMT-CI (lowest). Notably, while the shorter 94-nt insertion in the RMT-d2rep initially enhanced overall sgmRNA transcription and viral replication at earlier stages like 189-nt insertion, this broad enhancement for all sgmRNA was not sustained at later stages for unknown reasons (Figures 3, 4 and 6).

The first possible reason for the increased IFN induction in the mutant virus-infected cells is likely elevated production of aberrant (-)sgRNA intermediates, which potentially activated pattern recognition receptors such as RIG-I and MDA5 [68–70]. Consistent with this, several previous studies reported that the accumulation of (-)sgRNAs in SARS-CoV-2 infection correlated with increased IFN expression [71,72]. In our study, the restoration of sgmRNA hierarchy by the 189-nt insertion correlated with reduced IFN induction, supporting the idea that transcriptional accuracy helps suppress excessive innate immune responses. Alternatively, the translation of certain non-canonic sgmRNAs may be possible and the synthesized peptides can stimulate strong IFN responses. For example, we identified two abundant non-canonical sgmRNAs in all PEDV mutants carrying the remodeled TRS-CS with junctions near nucleotide 21111 and nucleotide 21166 (Table S1). This raises the possibility that remodeling the TRS-CS may inadvertently enable the translation of novel or frameshifted proteins. The third possible factor contributing to the increased IFN responses is the significantly reduced expression level of structural proteins after TRS remodeling, especially N protein, as suggested by transcription levels. With the 189-nt insertion, the reduced levels of S, M, N

 doi:10.20944/preprints202509.1182.v1

gene were compensated, and the E gene level was significantly enhanced. Notably, PEDV E protein have been implicated in IFN antagonism, and previous work showed that a PEDV mutant with an incomplete E protein induced higher IFN responses in vitro [73]. CoV N protein is also well known for suppressing host IFN responses [49,74,75]. This mechanistic link between TRS mutations, altered sgRNA/sgmRNA transcription profile, and IFN induction has potential pathophysiological significance, as IFNλ signaling is known to contribute to intestinal chloride dysregulation and diarrhea during viral enteritis [76]. And the diarrhea induction regulated by IFN signaling was suggested as an active host defense strategy to expel and eliminate the pathogen. Indeed, our previous in vivo data showed that both RMT and dORF3-EGFP exhibited similarly attenuated phenotypes in gnotobiotic (Gn) pigs, with generally moderate diarrhea [36]. Notably, some RMT-infected piglets still had transient severe diarrhea, whereas those infected with dORF3-EGFP did not. However, another study showed that the RMTv1 mutant, which was derived from RMT-CID with the EGFP gene deleted and induced similar IFN levels to RMT-CID in vitro (Figure S1), caused severe diarrhea in 100% Gn pigs [37]. These findings suggest that transcriptional inaccuracy and the resulting immune dysregulation may be associated with the elevated PEDV-induced diarrhea in this model.

Beyond transcriptional regulation, these findings have important implications for the development of live attenuated vaccines (LAVs) against CoVs and other nidoviruses [36–38,54,77]. Remodeling TRS-CSs can increase resistance to recombination but may result in potential transcriptional dysregulation and increased IFN responses. Incorporation of structured regulatory elements, such as the 189-nt insertion, may mitigate these drawbacks by enhancing sgmRNA expression while preserving attenuation. Moreover, although the 189-nt insertion enhanced all the structure protein sgmRNA transcription, it had the greatest effects on sgmRNA-E, whose ORF is immediately downstream of the insertion. While the PEDV E protein is less immunogenic [78], strategically positioning such regulatory elements upstream of highly immunogenic genes (e.g., S or N) could boost antigen expression and immunogenicity, improving vaccine efficacy. Additionally, the overexpression models provided by RMT or RMTd2rep offer novel platforms to study CoV E protein function, complementing prior loss-of-function approaches [73,79–81].

5. Conclusions

In summary, our study demonstrates that remodeling of the TRS-CS of PEDV impairs transcriptional accuracy, alters sgmRNA profiles and viral replication dynamics, and enhances IFN responses. The 189-nt insertion upstream of the E gene TRS-CS mitigates these detrimental defects, likely by promoting TRS pairing through structure-mediated mechanisms. These findings highlight the importance of incorporating both structural and functional considerations into TRS engineering for the development of recombination-resistant LAVs. Moreover, they provide new insights into the regulation of discontinuous transcription in CoVs and other nidoviruses that rely on TRS-regulated mechanisms.

Supplementary Materials: The following supporting information can be downloaded at the website of this paper posted on Preprints.org. Figure S1: Induction of type I and type III IFN mRNAs by the RMTv1 and RMT-CID in LLC-PK1 cells; Table S1: Special junctions of RMT.

Author Contributions: Conceptualization, M.L. and Q.W.; methodology/validation/investigation, M.L. and Q.W.; formal analysis/data curation, M.L., J.W.P., S.Y. and Q.W.; writing—original draft preparation, M.L. and Q.W.; writing—review and editing, M.L., J.W.P., S.Y., and Q.W.; visualization, M.L., J.W.P.; supervision/project administration/funding acquisition, Q.W. All authors have read and agreed to the published version of the manuscript.

 doi:10.20944/preprints202509.1182.v1

Funding: The project was supported by the National Institute of Food and Agriculture, U.S. Department of Agriculture, under award 2019-67015-29843 (Q.W., principal investigator).

Data Availability Statement: The data supporting the findings of this study are available within this article and the supplementary materials. Sequence reads generated in this study have been submitted to the NCBI SRA database under BioProject accession No. PRJNA1271575. The modified viral genome sequence is available upon request.

Acknowledgments: We thank Drs. Linda J. Saif, Anastasia Vlasova, and Scott Kenney for their critical suggestions for this project.

Conflicts of Interest: The authors declare no conflicts of interest. The funders had no role in the design of the study; in the collection, analyses, or interpretation of data; in the writing of the manuscript; or in the decision to publish the results.

Abbreviations

The following abbreviations are used in this manuscript:

CoV	coronaviruses
PEDV	porcine epidemic diarrhea virus
TRS-CS	transcription regulatory sequences- core sequences
gRNA	genomic RNA
sgmRNA	subgenomic messenger RNA
RMT	ReModel-Trs mutant
RMT-CI	RMT-Corrected Insertion
RMT-CID	RMT- Corrected Insertion and Deletion
RMT-d2rep	RMT-delete 2 repeats

References

1. Deng, X.; Baker, S.C. Coronaviruses: Molecular Biology (Coronaviridae). *Encyclopedia of Virology* **2021**, 198–207, doi:10.1016/B978-0-12-814515-9.02550-9.
2. Vlasova, A.N.; Kenney, S.P.; Jung, K.; Wang, Q.; Saif, L.J. Deltacoronavirus Evolution and Transmission: Current Scenario and Evolutionary Perspectives. *Frontiers in Veterinary Science* **2021**, *7*, 1257, doi:10.3389/fvets.2020.626785.
3. Peiris, J.S.M.; Lai, S.T.; Poon, L.L.M.; Guan, Y.; Yam, L.Y.C.; Lim, W.; Nicholls, J.; Yee, W.K.S.; Yan, W.W.; Cheung, M.T.; et al. Coronavirus as a Possible Cause of Severe Acute Respiratory Syndrome. *Lancet* **2003**, *361*, 1319–1325, doi:10.1016/s0140-6736(03)13077-2.
4. Zaki, A.M.; Boheemen, S. van; Bestebroer, T.M.; Osterhaus, A.D.M.E.; Fouchier, R.A.M. Isolation of a Novel Coronavirus from a Man with Pneumonia in Saudi Arabia. *New England Journal of Medicine* **2012**, *367*, 1814–1820, doi:10.1056/NEJMoa1211721.
5. Wu, F.; Zhao, S.; Yu, B.; Chen, Y.-M.; Wang, W.; Song, Z.-G.; Hu, Y.; Tao, Z.-W.; Tian, J.-H.; Pei, Y.-Y.; et al. Author Correction: A New Coronavirus Associated with Human Respiratory Disease in China. *Nature* **2020**, *580*, E7–E7, doi:10.1038/s41586-020-2202-3.
6. Zhu, N.; Zhang, D.; Wang, W.; Li, X.; Yang, B.; Song, J.; Zhao, X.; Huang, B.; Shi, W.; Lu, R.; et al. A Novel Coronavirus from Patients with Pneumonia in China, 2019. *New England Journal of Medicine* **2020**, *382*, 727–733, doi:10.1056/NEJMoa2001017.
7. Zhou, P.; Yang, X.-L.; Wang, X.-G.; Hu, B.; Zhang, L.; Zhang, W.; Si, H.-R.; Zhu, Y.; Li, B.; Huang, C.-L.; et al. A Pneumonia Outbreak Associated with a New Coronavirus of Probable Bat Origin. *Nature* **2020**, *579*, 270–273, doi:10.1038/s41586-020-2012-7.
8. Decaro, N.; Lorusso, A. Novel Human Coronavirus (SARS-CoV-2): A Lesson from Animal Coronaviruses. *Veterinary Microbiology* **2020**, *244*, 108693, doi:10.1016/j.vetmic.2020.108693.
9. Wood, EN. An Apparently New Syndrome of Porcine Epidemic Diarrhoea. *Vet. Rec.* **1977**, *100*, 243–244.

 doi:10.20944/preprints202509.1182.v1

10. Kong, F.; Jia, H.; Xiao, Q.; Fang, L.; Wang, Q. Prevention and Control of Swine Enteric Coronaviruses in China: A Review of Vaccine Development and Application. *Vaccines* **2024**, *12*, 11, doi:10.3390/vaccines12010011.
11. Li, W.; Li, H.; Liu, Y.; Pan, Y.; Deng, F.; Song, Y.; Tang, X.; He, Q. New Variants of Porcine Epidemic Diarrhea Virus, China, 2011. *Emerg Infect Dis* **2012**, doi:10.3201/eid1808.120002.
12. Jung, K.; Saif, L.J.; Wang, Q. Porcine Epidemic Diarrhea Virus (PEDV): An Update on Etiology, Transmission, Pathogenesis, and Prevention and Control. *Virus Res* **2020**, *286*, 198045, doi:10.1016/j.virusres.2020.198045.
13. Thomas, J.T.; Chen, Q.; Gauger, P.C.; Giménez-Lirola, L.G.; Sinha, A.; Harmon, K.M.; Madson, D.M.; Burrough, E.R.; Magstadt, D.R.; Salzbrenner, H.M.; et al. Effect of Porcine Epidemic Diarrhea Virus Infectious Doses on Infection Outcomes in Naïve Conventional Neonatal and Weaned Pigs. *PLoS One* **2015**, *10*, e0139266, doi:10.1371/journal.pone.0139266.
14. Liu, X.; Lin, C.-M.; Annamalai, T.; Gao, X.; Lu, Z.; Esseili, M.A.; Jung, K.; El-Tholoth, M.; Saif, L.J.; Wang, Q. Determination of the Infectious Titer and Virulence of an Original US Porcine Epidemic Diarrhea Virus PC22A Strain. *Vet Res* **2015**, *46*, 109, doi:10.1186/s13567-015-0249-1.
15. Sun, R.-Q.; Cai, R.-J.; Chen, Y.-Q.; Liang, P.-S.; Chen, D.-K.; Song, C.-X. Outbreak of Porcine Epidemic Diarrhea in Suckling Piglets, China. *Emerg Infect Dis* **2012**, doi:10.3201/eid1801.111259.
16. Schulz, L.L.; Tonsor, G.T. Assessment of the Economic Impacts of Porcine Epidemic Diarrhea Virus in the United States. *Journal of Animal Science* **2015**, *93*, 5111–5118, doi:10.2527/jas.2015-9136.
17. Song, D.; Park, B. Porcine Epidemic Diarrhoea Virus: A Comprehensive Review of Molecular Epidemiology, Diagnosis, and Vaccines. *Virus Genes* **2012**, *44*, 167–175, doi:10.1007/s11262-012-0713-1.
18. Niu, X.; Wang, Q. Prevention and Control of Porcine Epidemic Diarrhea: The Development of Recombination-Resistant Live Attenuated Vaccines. *Viruses* **2022**, *14*, 1317, doi:10.3390/v14061317.
19. Wang, Q.; Vlasova, A.N.; Kenney, S.P.; Saif, L.J. Emerging and Re-Emerging Coronaviruses in Pigs. *Curr Opin Virol* **2019**, *34*, 39–49, doi:10.1016/j.coviro.2018.12.001.
20. Pasternak, A.O.; Spaan, W.J.M.; Snijder, E.J. Nidovirus Transcription: How to Make Sense…? *Journal of General Virology* **2006**, *87*, 1403–1421, doi:10.1099/vir.0.81611-0.
21. Hou, Y.; Lin, C.-M.; Yokoyama, M.; Yount, B.L.; Marthaler, D.; Douglas, A.L.; Ghimire, S.; Qin, Y.; Baric, R.S.; Saif, L.J.; et al. Deletion of a 197-Amino-Acid Region in the N-Terminal Domain of Spike Protein Attenuates Porcine Epidemic Diarrhea Virus in Piglets. *Journal of Virology* **2017**, *91*, doi:10.1128/JVI.00227-17.
22. Beall, A.; Yount, B.; Lin, C.-M.; Hou, Y.; Wang, Q.; Saif, L.; Baric, R. Characterization of a Pathogenic Full-Length cDNA Clone and Transmission Model for Porcine Epidemic Diarrhea Virus Strain PC22A. *mBio* **2016**, *7*, doi:10.1128/mBio.01451-15.
23. Pensaert, MB.; De Bouck, P. A New Coronavirus-like Particle Associated with Diarrhea in Swine. *Archives of Virology* **1978**, *58*, 243–247, doi:10.1007/BF01317606.
24. Egberink, H.F.; Ederveen, J.; Callebaut, P.; Horzinek, M.C. Characterization of the Structural Proteins of Porcine Epizootic Diarrhea Virus, Strain CV777. *Am J Vet Res* **1988**, *49*, 1320–1324.
25. Sawicki, S.G.; Sawicki, D.L. Coronaviruses Use Discontinuous Extension for Synthesis of Subgenome-Length Negative Strands. *Adv Exp Med Biol* **1995**, *380*, 499–506, doi:10.1007/978-1-4615-1899-0_79.
26. Sawicki, S.G.; Sawicki, D.L. A New Model for Coronavirus Transcription. *Adv Exp Med Biol* **1998**, *440*, 215–219, doi:10.1007/978-1-4615-5331-1_26.
27. Sawicki, S.G.; Sawicki, D.L.; Siddell, S.G. A Contemporary View of Coronavirus Transcription. *Journal of Virology* **2007**, *81*, 20–29, doi:10.1128/JVI.01358-06.
28. Sola, I.; Almazán, F.; Zúñiga, S.; Enjuanes, L. Continuous and Discontinuous RNA Synthesis in Coronaviruses. *Annu. Rev. Virol.* **2015**, *2*, 265–288, doi:10.1146/annurev-virology-100114-055218.
29. Sola, I.; Moreno, J.L.; Zúñiga, S.; Alonso, S.; Enjuanes, L. Role of Nucleotides Immediately Flanking the Transcription-Regulating Sequence Core in Coronavirus Subgenomic mRNA Synthesis. *J Virol* **2005**, *79*, 2506–2516, doi:10.1128/JVI.79.4.2506-2516.2005.
30. Zúñiga, S.; Sola, I.; Alonso, S.; Enjuanes, L. Sequence Motifs Involved in the Regulation of Discontinuous Coronavirus Subgenomic RNA Synthesis. *J Virol* **2004**, *78*, 980–994, doi:10.1128/jvi.78.2.980-994.2004.

 doi:10.20944/preprints202509.1182.v1

31. Sola, I.; Mateos-Gomez, P.A.; Almazan, F.; Zuñiga, S.; Enjuanes, L. RNA-RNA and RNA-Protein Interactions in Coronavirus Replication and Transcription. *RNA Biology* **2011**, *8*, 237–248, doi:10.4161/rna.8.2.14991.
32. Alonso, S.; Izeta, A.; Sola, I.; Enjuanes, L. Transcription Regulatory Sequences and mRNA Expression Levels in the Coronavirus Transmissible Gastroenteritis Virus. *J Virol* **2002**, *76*, 1293–1308, doi:10.1128/jvi.76.3.1293-1308.2002.
33. Mori, A.; Lavezzari, D.; Pomari, E.; Deiana, M.; Piubelli, C.; Capobianchi, M.R.; Castilletti, C. sgRNAs: A SARS-CoV-2 Emerging Issue. *Aspects of Molecular Medicine* **2023**, *1*, 100008, doi:10.1016/j.amolm.2023.100008.
34. Kim, D.; Lee, J.-Y.; Yang, J.-S.; Kim, J.W.; Kim, V.N.; Chang, H. The Architecture of SARS-CoV-2 Transcriptome. *Cell* **2020**, *181*, 914-921.e10, doi:10.1016/j.cell.2020.04.011.
35. Wang, D.; Jiang, A.; Feng, J.; Li, G.; Guo, D.; Sajid, M.; Wu, K.; Zhang, Q.; Ponty, Y.; Will, S.; et al. The SARS-CoV-2 Subgenome Landscape and Its Novel Regulatory Features. *Molecular Cell* **2021**, doi:10.1016/j.molcel.2021.02.036.
36. Niu, X.; Liu, M.; Yang, S.; Xu, J.; Hou, Y.J.; Liu, D.; Tang, Q.; Zhu, H.; Wang, Q. A Recombination-Resistant Genome for Live Attenuated and Stable PEDV Vaccines by Engineering the Transcriptional Regulatory Sequences. *Journal of Virology* **2023**, *0*, e01193-23, doi:10.1128/jvi.01193-23.
37. Liu, M.; Aryal, B.; Niu, X.; Wang, Q. Engineering a Recombination-Resistant Live Attenuated Vaccine Candidate with Suppressed Interferon Antagonists for PEDV. *Journal of Virology* **2025**.
38. Li, L.; Chen, J.; Cao, Z.; Guo, Z.; Liu, J.; Zhou, Y.; Tong, G.; Gao, F. Engineering a Live-Attenuated Porcine Reproductive and Respiratory Syndrome Virus Vaccine to Prevent RNA Recombination by Rewiring Transcriptional Regulatory Sequences. *mBio* **2024**, *0*, e02350-24, doi:10.1128/mbio.02350-24.
39. Yount, B.; Roberts, R.S.; Lindesmith, L.; Baric, R.S. Rewiring the Severe Acute Respiratory Syndrome Coronavirus (SARS-CoV) Transcription Circuit: Engineering a Recombination-Resistant Genome. *Proceedings of the National Academy of Sciences* **2006**, *103*, 12546–12551, doi:10.1073/pnas.0605438103.
40. Oka, T.; Saif, L.J.; Marthaler, D.; Esseili, M.A.; Meulia, T.; Lin, C.-M.; Vlasova, A.N.; Jung, K.; Zhang, Y.; Wang, Q. Cell Culture Isolation and Sequence Analysis of Genetically Diverse US Porcine Epidemic Diarrhea Virus Strains Including a Novel Strain with a Large Deletion in the Spike Gene. *Veterinary microbiology* **2014**, *173*, 258–269.
41. Niu, X.; Kong, F.; Xu, J.; Liu, M.; Wang, Q. Mutations in Porcine Epidemic Diarrhea Virus Nsp1 Cause Increased Viral Sensitivity to Host Interferon Responses and Attenuation In Vivo. *Journal of Virology* **2022**, *96*, e00469-22, doi:10.1128/jvi.00469-22.
42. Hou, Y.; Ke, H.; Kim, J.; Yoo, D.; Su, Y.; Boley, P.; Chepngeno, J.; Vlasova, A.N.; Saif, L.J.; Wang, Q. Engineering a Live Attenuated PEDV Vaccine Candidate via Inactivation of the Viral 2′-O Methyltransferase and the Endocytosis Signal of the Spike Protein. *Journal of Virology* **2019**, doi:10.1128/JVI.00406-19.
43. Zuker, M. Mfold Web Server for Nucleic Acid Folding and Hybridization Prediction. *Nucleic Acids Research* **2003**, *31*, 3406–3415, doi:10.1093/nar/gkg595.
44. Xu, J.; Liu, M.; Niu, X.; Hanson, J.; Jung, K.; Ru, P.; Tu, H.; Jones, D.M.; Vlasova, A.N.; Saif, L.J.; et al. The Cold-Adapted, Temperature-Sensitive SARS-CoV-2 Strain TS11 Is Attenuated in Syrian Hamsters and a Candidate Attenuated Vaccine. *Viruses* **2023**, *15*, 95, doi:10.3390/v15010095.
45. Reed, L.J.; Muench, H. A SIMPLE METHOD OF ESTIMATING FIFTY PER CENT ENDPOINTS12. *American Journal of Epidemiology* **1938**, *27*, 493–497, doi:10.1093/oxfordjournals.aje.a118408.
46. Sotcheff, S.; Zhou, Y.; Yeung, J.; Sun, Y.; Johnson, J.E.; Torbett, B.E.; Routh, A.L. ViReMa: A Virus Recombination Mapper of next-Generation Sequencing Data Characterizes Diverse Recombinant Viral Nucleic Acids. *Gigascience* **2023**, *12*, giad009, doi:10.1093/gigascience/giad009.
47. Kong, F.; Niu, X.; Liu, M.; Wang, Q. Bile Acids LCA and CDCA Inhibited Porcine Deltacoronavirus Replication in Vitro. *Vet Microbiol* **2021**, *257*, 109097, doi:10.1016/j.vetmic.2021.109097.
48. Livak, K.J.; Schmittgen, T.D. Analysis of Relative Gene Expression Data Using Real-Time Quantitative PCR and the 2(-Delta Delta C(T)) Method. *Methods* **2001**, *25*, 402–408, doi:10.1006/meth.2001.1262.

 doi:10.20944/preprints202509.1182.v1

49. Ding, Z.; Fang, L.; Jing, H.; Zeng, S.; Wang, D.; Liu, L.; Zhang, H.; Luo, R.; Chen, H.; Xiao, S. Porcine Epidemic Diarrhea Virus Nucleocapsid Protein Antagonizes Beta Interferon Production by Sequestering the Interaction between IRF3 and TBK1. *J Virol* **2014**, *88*, 8936–8945, doi:10.1128/JVI.00700-14.
50. Xu, X.; Zhang, H.; Zhang, Q.; Huang, Y.; Dong, J.; Liang, Y.; Liu, H.-J.; Tong, D. Porcine Epidemic Diarrhea Virus N Protein Prolongs S-Phase Cell Cycle, Induces Endoplasmic Reticulum Stress, and up-Regulates Interleukin-8 Expression. *Vet Microbiol* **2013**, *164*, 212–221, doi:10.1016/j.vetmic.2013.01.034.
51. Hao, L.; Fragoso-Saavedra, M.; Liu, Q. Upregulation of Porcine Epidemic Diarrhea Virus (PEDV) RNA Translation by the Nucleocapsid Protein. *Virology* **2025**, *602*, 110306, doi:10.1016/j.virol.2024.110306.
52. Wrapp, D.; McLellan, J.S. The 3.1-Angstrom Cryo-Electron Microscopy Structure of the Porcine Epidemic Diarrhea Virus Spike Protein in the Prefusion Conformation. *J Virol* **2019**, *93*, e00923-19, doi:10.1128/JVI.00923-19.
53. Bosch, B.J.; van der Zee, R.; de Haan, C.A.M.; Rottier, P.J.M. The Coronavirus Spike Protein Is a Class I Virus Fusion Protein: Structural and Functional Characterization of the Fusion Core Complex. *J Virol* **2003**, *77*, 8801–8811, doi:10.1128/jvi.77.16.8801-8811.2003.
54. Graham, R.L.; Deming, D.J.; Deming, M.E.; Yount, B.L.; Baric, R.S. Evaluation of a Recombination-Resistant Coronavirus as a Broadly Applicable, Rapidly Implementable Vaccine Platform. *Commun Biol* **2018**, *1*, 1–10, doi:10.1038/s42003-018-0175-7.
55. Liu, Y.; Zhang, X.; Liu, J.; Xia, H.; Zou, J.; Muruato, A.E.; Periasamy, S.; Kurhade, C.; Plante, J.A.; Bopp, N.E.; et al. A Live-Attenuated SARS-CoV-2 Vaccine Candidate with Accessory Protein Deletions. *Nat Commun* **2022**, *13*, 4337, doi:10.1038/s41467-022-31930-z.
56. Yang, Y.; Yan, W.; Hall, A.B.; Jiang, X. Characterizing Transcriptional Regulatory Sequences in Coronaviruses and Their Role in Recombination. *Molecular Biology and Evolution* **2021**, *38*, 1241–1248, doi:10.1093/molbev/msaa281.
57. Boniotti, M.B.; Papetti, A.; Lavazza, A.; Alborali, G.; Sozzi, E.; Chiapponi, C.; Faccini, S.; Bonilauri, P.; Cordioli, P.; Marthaler, D. Porcine Epidemic Diarrhea Virus and Discovery of a Recombinant Swine Enteric Coronavirus, Italy. *Emerg Infect Dis* **2016**, *22*, 83–87, doi:10.3201/eid2201.150544.
58. Leary, S.; Gaudieri, S.; Parker, M.D.; Chopra, A.; James, I.; Pakala, S.; Alves, E.; John, M.; Lindsey, B.B.; Keeley, A.J.; et al. Generation of a Novel SARS-CoV-2 Sub-Genomic RNA Due to the R203K/G204R Variant in Nucleocapsid: Homologous Recombination Has Potential to Change SARS-CoV-2 at Both Protein and RNA Level. *Pathog Immun* **2021**, *6*, 27–49, doi:10.20411/pai.v6i2.460.
59. Mears, H.V.; Young, G.R.; Sanderson, T.; Harvey, R.; Barrett-Rodger, J.; Penn, R.; Cowton, V.; Furnon, W.; Lorenzo, G.D.; Crawford, M.; et al. Emergence of SARS-CoV-2 Subgenomic RNAs That Enhance Viral Fitness and Immune Evasion. *PLOS Biology* **2025**, *23*, e3002982, doi:10.1371/journal.pbio.3002982.
60. Duguay, B.A.; Tooley, T.H.; Pringle, E.S.; Rohde, J.R.; McCormick, C. A Yeast-Based Reverse Genetics System to Generate HCoV-OC43 Reporter Viruses Encoding an Eighth Subgenomic RNA. *Journal of Virology* **2025**, *99*, e01671-24, doi:10.1128/jvi.01671-24.
61. Stombaugh, J.; Zirbel, C.L.; Westhof, E.; Leontis, N.B. Frequency and Isostericity of RNA Base Pairs. *Nucleic Acids Res* **2009**, *37*, 2294–2312, doi:10.1093/nar/gkp011.
62. Bresson, S.; Sani, E.; Armatowska, A.; Dixon, C.; Tollervey, D. The Transcriptional and Translational Landscape of HCoV-OC43 Infection. *PLOS Pathogens* **2025**, *21*, e1012831, doi:10.1371/journal.ppat.1012831.
63. Dufour, D.; Mateos-Gomez, P.A.; Enjuanes, L.; Gallego, J.; Sola, I. Structure and Functional Relevance of a Transcription-Regulating Sequence Involved in Coronavirus Discontinuous RNA Synthesis. *Journal of Virology* **2011**, *85*, 4963–4973, doi:10.1128/jvi.02317-10.
64. Shang, P.; Li, Y.; Napthine, S.; Chen, C.; Brierley, I.; Firth, A.E.; Fang, Y. An Intra-Family Conserved High-Order RNA Structure within the M ORF Is Important for Arterivirus Subgenomic RNA Accumulation and Infectious Virus Production. *Journal of Virology* **2025**, *0*, e02167-24, doi:10.1128/jvi.02167-24.
65. Zhang, Y.; Huang, K.; Xie, D.; Lau, J.Y.; Shen, W.; Li, P.; Wang, D.; Zou, Z.; Shi, S.; Ren, H.; et al. In Vivo Structure and Dynamics of the SARS-CoV-2 RNA Genome. *Nat Commun* **2021**, *12*, 5695, doi:10.1038/s41467-021-25999-1.
66. Madhugiri, R.; Nguyen, H.V.; Slanina, H.; Ziebuhr, J. Alpha- and Betacoronavirus *Cis*-Acting RNA Elements. *Current Opinion in Microbiology* **2024**, *79*, 102483, doi:10.1016/j.mib.2024.102483.

 doi:10.20944/preprints202509.1182.v1

67. Wu, Z.-C.; Xia, X.-J.; Li, H.-R.; Jiang, S.-J.; Ma, Z.-Y.; Wang, X. Tandem Repeat Sequence of Duck Circovirus Serves as Downstream Sequence Element to Regulate Viral Gene Expression. *Veterinary Microbiology* **2019**, *239*, 108496, doi:10.1016/j.vetmic.2019.108496.
68. Loo, Y.-M.; Fornek, J.; Crochet, N.; Bajwa, G.; Perwitasari, O.; Martinez-Sobrido, L.; Akira, S.; Gill, M.A.; García-Sastre, A.; Katze, M.G.; et al. Distinct RIG-I and MDA5 Signaling by RNA Viruses in Innate Immunity. *J Virol* **2008**, *82*, 335–345, doi:10.1128/JVI.01080-07.
69. Rehwinkel, J.; Gack, M.U. RIG-I-like Receptors: Their Regulation and Roles in RNA Sensing. *Nat Rev Immunol* **2020**, *20*, 537–551, doi:10.1038/s41577-020-0288-3.
70. Yamada, T.; Takaoka, A. Innate Immune Recognition against SARS-CoV-2. *Inflamm Regener* **2023**, *43*, 7, doi:10.1186/s41232-023-00259-5.
71. Zhao, Y.; Sun, J.; Li, Y.; Li, Z.; Xie, Y.; Feng, R.; Zhao, J.; Hu, Y. The Strand-Biased Transcription of SARS-CoV-2 and Unbalanced Inhibition by Remdesivir. *iScience* **2021**, *24*, doi:10.1016/j.isci.2021.102857.
72. Zhang, Y.; Zhang, X.; Zheng, H.; Liu, L. Subgenomic RNAs and Their Encoded Proteins Contribute to the Rapid Duplication of SARS-CoV-2 and COVID-19 Progression. *Biomolecules* **2022**, *12*, 1680, doi:10.3390/biom12111680.
73. Li, Z.; Ma, Z.; Han, W.; Chang, C.; Li, Y.; Guo, X.; Zheng, Z.; Feng, Y.; Xu, L.; Zheng, H.; et al. Deletion of a 7-Amino-Acid Region in the Porcine Epidemic Diarrhea Virus Envelope Protein Induces Higher Type I and III Interferon Responses and Results in Attenuation in Vivo. *J Virol* **2023**, *97*, e0084723, doi:10.1128/jvi.00847-23.
74. Kim, Y.-M.; Shin, E.-C. Type I and III Interferon Responses in SARS-CoV-2 Infection. *Exp Mol Med* **2021**, *53*, 750–760, doi:10.1038/s12276-021-00592-0.
75. Chen, K.; Xiao, F.; Hu, D.; Ge, W.; Tian, M.; Wang, W.; Pan, P.; Wu, K.; Wu, J. SARS-CoV-2 Nucleocapsid Protein Interacts with RIG-I and Represses RIG-Mediated IFN-β Production. *Viruses* **2021**, *13*, 47, doi:10.3390/v13010047.
76. Hou, G.; Son, J.; Gomez Castro, M.F.; Kawagishi, T.; Ren, X.; Roth, A.N.; Antia, A.; Zeng, Q.; DeVeaux, A.L.; Feng, N.; et al. Innate Immune Sensing of Rotavirus by Intestinal Epithelial Cells Leads to Diarrhea. *Cell Host Microbe* **2025**, S1931-3128(25)00053-8, doi:10.1016/j.chom.2025.02.005.
77. Liu, Y.; Zhang, X.; Liu, J.; Xia, H.; Zou, J.; Muruato, A.E.; Periasamy, S.; Plante, J.A.; Bopp, N.E.; Kurhade, C.; et al. A Live-Attenuated SARS-CoV-2 Vaccine Candidate with Accessory Protein Deletions 2022, 2022.02.14.480460.
78. Gimenez-Lirola, L.G.; Zhang, J.; Carrillo-Avila, J.A.; Chen, Q.; Magtoto, R.; Poonsuk, K.; Baum, D.H.; Piñeyro, P.; Zimmerman, J. Reactivity of Porcine Epidemic Diarrhea Virus Structural Proteins to Antibodies against Porcine Enteric Coronaviruses: Diagnostic Implications. *J Clin Microbiol* **2017**, *55*, 1426–1436, doi:10.1128/JCM.02507-16.
79. Nieto-Torres, J.L.; DeDiego, M.L.; Verdiá-Báguena, C.; Jimenez-Guardeño, J.M.; Regla-Nava, J.A.; Fernandez-Delgado, R.; Castaño-Rodriguez, C.; Alcaraz, A.; Torres, J.; Aguilella, V.M.; et al. Severe Acute Respiratory Syndrome Coronavirus Envelope Protein Ion Channel Activity Promotes Virus Fitness and Pathogenesis. *PLOS Pathogens* **2014**, *10*, e1004077, doi:10.1371/journal.ppat.1004077.
80. Castaño-Rodriguez, C.; Honrubia, J.M.; Gutiérrez-Álvarez, J.; DeDiego, M.L.; Nieto-Torres, J.L.; Jimenez-Guardeño, J.M.; Regla-Nava, J.A.; Fernandez-Delgado, R.; Verdia-Báguena, C.; Queralt-Martín, M.; et al. Role of Severe Acute Respiratory Syndrome Coronavirus Viroporins E, 3a, and 8a in Replication and Pathogenesis. *mBio* **2018**, *9*, 10.1128/mbio.02325-17, doi:10.1128/mbio.02325-17.
81. Kuo, L.; Masters, P.S. The Small Envelope Protein E Is Not Essential for Murine Coronavirus Replication. *Journal of Virology* **2003**, *77*, 4597–4608, doi:10.1128/jvi.77.8.4597-4608.2003.